HHS Public Access

Author manuscript

J Neural Eng. Author manuscript; available in PMC 2019 June 01.

Published in final edited form as:

J Neural Eng. 2018 June 01; 15(3): 036027–. doi:10.1088/1741-2552/aab55f.

Flexible microelectrode array for interfacing with the surface of neural ganglia

Zachariah J Sperry[1,2], **Kyoungwhan Na**[3], **Saman S Parizi**[3], **Hillel J. Chiel**[4,5,6], **John Seymour**[1,3], **Euisik Yoon**[1,3], and **Tim M Bruns**[1,2]

[1]Biomedical Engineering, University of Michigan, Ann Arbor, MI

[2]Biointerfaces Institute, University of Michigan, Ann Arbor, MI

[3]Electrical Engineering and Computer Science, University of Michigan, Ann Arbor, MI

[4]Biology, Case Western Reserve University, Cleveland, OH

[5]Neurosciences, Case Western Reserve University, Cleveland, OH

[6]Biomedical Engineering, Case Western Reserve University, Cleveland, OH

Abstract

Objective—The dorsal root ganglia (DRG) are promising nerve structures for sensory neural interfaces because they provide centralized access to primary afferent cell bodies and spinal reflex circuitry. In order to harness this potential, new electrode technologies are needed which take advantage of the unique properties of DRG, specifically the high density of neural cell bodies at the dorsal surface. Here we report initial *in vivo* results from the development of a flexible non-penetrating polyimide electrode array interfacing with the surface of ganglia.

Approach—Multiple layouts of a 64-channel iridium electrode (420 μm^2) array were tested, with pitch as small as 25 μm. The buccal ganglia of invertebrate sea slug *Aplysia californica* were used to develop handling and recording techniques with ganglionic surface electrode arrays (GSEAs). We also demonstrated the GSEA's capability to record single- and multi-unit activity from feline lumbosacral DRG related to a variety of sensory inputs, including cutaneous brushing, joint flexion, and bladder pressure.

Main results—We recorded action potentials from a variety of *Aplysia* neurons activated by nerve stimulation, and units were observed firing simultaneously on closely spaced electrode sites. We also recorded single- and multi-unit activity associated with sensory inputs from feline DRG. We utilized spatial oversampling of action potentials on closely-spaced electrode sites to estimate the location of neural sources at between 25 μm and 107 μm below the DRG surface. We also used the high spatial sampling to demonstrate a possible spatial sensory map of one feline's DRG. We obtained activation of sensory fibers with low-amplitude stimulation through individual or groups of GSEA electrode sites.

Significance—Overall, the GSEA has been shown to provide a variety of information types from ganglia neurons and to have significant potential as a tool for neural mapping and interfacing.

Keywords

microelectrode; DRG; dorsal root ganglia; feline; *Aplysia*; source localization; polyimide

Introduction

Dorsal root ganglia (DRG) are spinal root components that hold significant promise as neural interface sites, particularly for open- or closed-loop sensory neuroprostheses. DRG are elongated thickenings of the dorsal spinal roots at each spinal level that contain cell bodies for afferent neurons entering the spinal cord. Cell bodies are particularly useful for neural recording because of the large extracellular voltage fluctuation that occurs around the soma during action potential propagation [1]. Neural signaling involving these cell bodies often remains intact below the level of a spinal cord injury (SCI), so with a proper electrode interface it is possible to record and decode the sensory signals contained within the firing rates of the electrical impulses. Neural decoding has been previously demonstrated both acutely and chronically for monitoring skin sensation, limb position, and bladder pressure using penetrating microelectrode arrays inserted into DRG, sometimes as sensory feedback for stimulation applications [2]–[9].

As a therapeutic technique, a DRG neural interface has the potential to restore function to some of the approximately 17,000 patients who suffer an SCI each year [10]. While an SCI patient's most visible symptom may be limb paralysis, equal or higher priority is often given by patients to development of new therapies addressing impairment of respiratory, bladder, bowel, or sexual functions [11], [12]. Significant effort in the field of neural stimulation has been directed toward functional solutions for SCI patients, including functional electrical stimulation (FES) for direct activation of paralyzed muscles; epidural spinal stimulation for restoration of motor behavior; intracortical stimulation to restore natural touch perception; and stimulation for axonal regeneration [13]–[15]. Microstimulation of DRG could contribute to this effort by using the same neural interface technology for recording to activate primary somatosensory afferents, a step towards restoring sensation [16]–[19], and providing open-loop modulation of bladder pressure through activation of spinal reflex pathways [8], [20].

DRG interfaces also have value in advancing our understanding of neurophysiology. The physiology of complex autonomic and reflex circuits, such as those of the bladder and gut, involves many different neurons across several distinct nerves. Separately accessing each nerve for recording can be unwieldy. In contrast, the DRG at each spinal level serves as a nexus for multiple nerves and therefore allows interface with many different neurons from a single location. Recordings from single sacral feline DRG, for example, has benefited research into lower urinary tract physiology through access to both pelvic and pudendal afferents [8], [9], [21]. Further, some of the nerves and nerve plexi of the autonomic system (including the pelvic plexus) are challenging to interface with because of their very small size peripherally before they join at the spinal root. A DRG interface would mitigate this problem.

Despite the promise of such an interface, there are currently no technologies designed specifically for interfacing with the DRG's unique morphology. In the peripheral nervous system, interfacing is typically accomplished with different types of cuff electrodes, which encircle a nerve branch to insulate the tissue-electrode interface. The current technological

standard is a flexible split cylinder of fixed diameter which opens around a nerve and has electrode contacts (typically platinum, platinum/iridium, or stainless steel) on the interior surface [22]. This would be an impractical approach in the DRG, however, as it is surgically difficult to lift the DRG from its anatomical position within the spinal canal. The DRG also does not have a constant diameter, but tapers at either end into the spinal nerve. If the surgical problem is overcome, newer built-to-fit or self-sizing cuff designs could be used. In terms of signal quality, however, cuff electrodes typically present poor selectivity for individual fascicles or neurons [22]. The flat interface nerve electrode (FINE) cuff attempts to overcome this issue by gently reshaping the nerve profile from circular to roughly rectangular. With the fascicles arranged closer to the nerve surface, selectivity is improved for stimulation and for recording of compound action potentials [23]–[25]. While this design appears suitable for chronic peripheral nerve interfaces, based on 3-month implants in felines, it is unknown whether the reshaping approach could be adapted for the soma-containing DRG.

Most studies in DRG utilize micro-wires, Utah-style electrode arrays or floating microelectrode arrays, inserted into the tissue with a pneumatic insertion tool [1]–[8], [16]–[20], [26]. While effective for limited recording periods, these electrodes have several shortcomings. First, penetrating arrays have the potential to cause tissue damage and encapsulation. This has been shown in brain and peripheral nerves to be the result of damage caused by the initial insertion and, more importantly, by micromotion of the very stiff silicon electrodes relative to the neural tissue [27]–[29]. Chronic Utah array studies in DRG suggest a maximum lifetime of a few weeks to a few months, probably due to a greater degree of motion in the spine than in the cranium [8], [18]. The DRG has a curved surface, while the backing of Utah electrode arrays is flat. More importantly, it has been observed that the majority of DRG cell bodies are localized around the DRG periphery, particularly at the dorsal aspect below a sub-100 μm thick epineurium [30], [31]. While it may be possible to assemble short, stiff, multi-site silicon-based devices to access this population of neurons, it is likely that these would have difficulty penetrating through the thick epineurial layer.

These problems may be overcome with the application of a flexible non-penetrating interface. Recording neural activity from the surface of neural structures is a well-established technique. In the brain, micro-electroencephalogram (μ-ECoG) arrays shrink the size and spacing of standard ECoG technologies for recording from large neuron populations at the cortical brain surface. One novel approach to improve conformability to the brain surface was the application of a 2.5 μm-thick polyimide mesh array using dissolvable silk backing. This device was capable of recording optically evoked potentials, though the signal-to-noise ratio (SNR) was somewhat low so recordings had to be averaged [32]. Minev et al. presented a hybrid design for use on the surface of either brain or spinal cord, using a 120 μm-thick silicone substrate to achieve mechanical properties similar to the underlying neural tissue. This design, capable of ECoG recordings (motor cortex) and driving motor behavior through stimulation (lumbosacral spinal cord) was shown in chronically implanted rats to be superior to stiff 25 μm thick polyimide in terms of avoiding mechanical tissue damage, inflammatory response, and effect on animal motor performance. This study suggested that very thin polyimide, on the order of single microns, might share some of these advantages due to its mechanics [33]. Rodger et al. used a parylene array to record

somatosensory evoked potentials from mouse spinal cord, but the electrodes were not suitable for single-unit or multi-unit recording [34]. Polymer substrates serve as better mechanical matches to neural tissue and have been used for insertion into peripheral nerves as intrafascicular recording arrays [35]–[37]. Additionally, the biocompatibility benefits of thin flexible devices will continue to increase their prominence in the field of neurointerfaces, though issues of water intrusion, delamination, and securement will need to be solved for chronic use [38].

The shortcomings of standard arrays and increasing research in the application thin films for neural recording provide an opportunity for evaluation of a thin-film electrode arrays for DRG interface. In this study, we study a Ganglionic Surface Electrode Array (GSEA). Surface DRG recordings have been previously reported in both felines and humans [39]. The results were promising, demonstrating that it is possible to obtain single- and multi-unit neural recordings from the DRG surface. The devices used in that study, however, were adapted from other neural technologies not intended for DRG, which not only did not conform to the DRG surface but required application of active pressure to obtain recordings. This could be problematic in any experiment, particularly a chronically implanted system. Here, we demonstrate fabrication of a custom-designed interface for the DRG surface, having iridium electrodes embedded in a flexible polyimide substrate, and show that it is capable of recording single- and multi-unit sensory signals from the surface of feline lumbosacral DRG. We also utilized the buccal ganglia of *Aplysia californica* (Pacific sea slugs) as an important part of our electrode development and testing.

Methods

Ganglionic Surface Array (GSEA) Fabrication

The GSEA was fabricated in the Lurie Nanofabrication Facility at the University of Michigan. The process required four masks and used a 4” silicon wafer as the mechanical substrate. The device substrate was a thin, biostable PI made of BPDA-PDA (3,3’,4,4’-biphenyltetracarboxilic dianhydride with *p*-phenylene diamine) [38]. This variety of polyimide was chosen because of its high yield strength, flexibility, and low water absorption [40]. A lower polyimide layer, specifically PI-2610 (HD Microsystems, Wilmington, DE) was spun on at 2.2 μm thick. Lift-off patterning of thin metal interconnect lines allowed for 2.5-μm-wide traces with very high yield. Next the top polyimide layer was spun on, PI-2610 with the same thickness as the lower layer to place the metal traces in a neutral plane. A thin adhesion layer of titanium dioxide was also used above and below the metal stack. The outer structure of the arrays and the contact openings were patterned with a hard mask and O_2 plasma etching. Using liftoff patterning, a stack of titanium-platinum-iridium was deposited on the top of the polyimide array and into the contact to form the microelectrode metal interface. Both the O_2 etching step and the inclusion of titanium in the metal stack are based on improved metal-polymer adhesion reported by other groups [40]. Impedance of functional (<1 MΩ) 420-μm^2 sites was 515 ± 206 kΩ pre-implant in 10% saline and 503 ± 225 kΩ when applied to a nerve structure (measured using Ripple Grapevine system (Ripple LLC, Salt Lake City, UT)). Figure 1 shows the fabrication stack diagram, tested layouts, and an example GSEA.

In vitro Invertebrate Testing

The nervous systems of *Aplysia californica* serve as relatively simple and inexpensive models for testing neural technologies prior to and in parallel with vertebrate *in vivo* experiments [41], [42]. Like vertebrates, *Aplysia* have ganglia containing neural cell bodies and surrounded by connective tissue (~100 μm thick), though this tissue has somewhat different mechanical and electrical properties than vertebrate epineurium [43]. Surface-based multielectrode approaches have previously been used to record from invertebrate ganglia, though only stiff planar arrays have been demonstrated [44]–[46]. The buccal ganglia, responsible for both afferent and efferent innervation of the feeding apparatus, is a particularly well-studied component of the *Aplysia* nervous system and was the *in vitro* ganglia chosen for this study [47]–[49].

Aplysia californica were purchased from the NIH/University of Miami National Resource for Aplysia Facility (160 ± 50 g). Animals were housed in a 40-gallon saltwater tank at 16 °C. To isolate buccal ganglia, a single *Aplysia* was first anesthetized with one-half of its body volume in ~0.3 M $MgCl_2$. Incisions were made in the head region to expose the buccal mass, which contains the mouth parts and associated neural tissues including the buccal ganglia. The ganglia was pinned out in an agar or Sylgard-filled dish (Dow Corning, Auburn, MI) using insect pins, and the dish filled with an isotonic saline solution to just cover the ganglia.

A suction electrode, consisting of chloridized silver wire and isotonic saline inside 0.050 inch polyethylene tubing, was placed near the second buccal nerve, and a syringe was used to pull the nerve into the electrode. Electrical stimulation (Isolated Pulse Stimulator Model 2100, A-M Systems, Carlsborg, WA) through this electrode was used to elicit verified neural activity [50]. A GSEA was placed on the surface of the ganglia for recording action potentials through the Ripple Grapevine processor. In some experiments, a foam-tipped plastic spear was used to press the GSEA onto the surface of the ganglia.

The ganglia were stimulated electrically through the first suction electrode with square waveforms of varying frequencies and pulse-widths to elicit neural activity. Although a variety of stimulus signals were attempted, a typical stimulus was 2Hz, 300μA, 1ms biphasic pulse [50]. Signals were recorded using Ripple Trellis software.

In vivo Feline Testing

Intact, domestic, short-haired adult cats (Liberty Research, Inc., Waverly, NY) were used in non-survival experiments in this study with one cat used per experiment. All procedures were approved by the University of Michigan Institutional Animal Care and Use Committee, in accordance with the National Institute of Health's guidelines for the care and use of laboratory animals. Prior to use, animals were free-range housed with 0–3 fellow felines in a 413 ft^2 room with controlled temperature (19–21 °C) and relative humidity (35–60%), food and water available ad lib, and a 12 h light/dark cycle. Enrichment was provided by toys and daily staff interaction.

Animals were initially anesthetized with a ketamine (6.6 mg/kg)-butorphanol (0.66 mg/kg)-dexmedetomidine (0.033 mg/kg) intramuscular (IM) dose, intubated, and then maintained on

isoflurane anesthesia (2–4 %) during surgical procedures. Respiratory rate, heart rate, end-tidal CO_2, O_2 perfusion, temperature, and intra- arterial blood pressure were monitored continuously using a Surgivet vitals monitor (Smiths Medical, Dublin, OH). Intravenous (IV) lines were inserted into one or both cephalic veins for drug and fluid infusions. Intravenous fluids (1:1 ratio of lactated Ringers solution and 5 % dextrose) were infused at a rate of 5–10 mL/kg/h and increased up to 30 mL/kg/h during surgery as needed. Via a laparotomy, a dual-lumen suprapubic catheter was placed for bladder access. Following a medial incision over the lower lumbar and sacral spine, a laminectomy was performed to expose the lumbosacral spinal cord and DRG (typically L7-S2). Electrode impedances were measured prior to placement in 0.9% saline. A micromanipulator on a magnetic stand was used to support and position the GSEAs, which were lowered into place on the dorsal surface of different DRG, and impedance was taken again. No adhesive was used to secure the GSEAs, which were held down only by surface tension to the moist tissue or with manual pressure via a cotton or foam applicator. The reference wire was inserted into the intraspinal space or nearby muscle. The ground wire was connected to a 12 gauge stainless steel needle inserted under the skin on the left or right flank. With the GSEAs in various positions on the different DRG, neural activity was recorded at 30 kHz using the Ripple Grapevine NIP and associated Trellis software. We simultaneously monitored bladder pressure at 1 kHz through the bladder catheter with a pressure transducer (DPT-100, Utah Medical Products, Midvale, UT) and analog amplifier (SYS-TBM4M, World Precision Instruments, Sarasota, FL) also connected to the NIP for synchronization.

Various sensory stimuli were applied to activate a range of afferents, though not every kind of stimulus was used in every experiment. To activate skin afferents, the skin was brushed using a cotton applicator in the dermatome associated with the DRG of interest. For L7, this included different regions of the back and legs. For S1 and S2, this included regions of the tail, the anus, and the scrotum (for male cats) [2], [51]. These trials typically involved brushing in bouts of 10 s with 10 s rest periods between bouts. To activate proprioceptive afferents (L7 only), the ankle or knee joint was manually bent. To activate lower urinary tract afferents, room or body-temperature saline was infused through the indwelling catheter in separate boluses of 5 mL until 30 mL had been introduced. Any fluid not voided was removed from the bladder via the in-dwelling catheter.

In some experiments, electrical stimulation was applied (biphasic, 1:2 charge balanced, cathode-leading, 200 μs pulse-width) at low levels (15–300 μA, 7.5 μA resolution) to the DRG through one or more electrode channels, and the animal was observed for corresponding responses.

After completion of all testing, animals were euthanized with an intravenous dose of sodium pentobarbital (390 mg/mL) while under deep anesthesia, followed by bilateral pneumothorax.

Data Analysis

Single-unit action potential timing was calculated in Plexon Offline Sorter (Plexon, Dallas, TX) from the raw neural data by first digitally filtering (high-pass, 250 Hz) then manually applying a negative threshold slightly below the noise floor prior to manual sorting to

capture all potential units. For *Aplysia* recordings, spike windows of 3–6 ms were used due to the longer spike duration of these neurons relative to vertebrate action potentials, for which 1.7 ms windows were used. Detected spikes were manually sorted out from noise signals, aided by principal component analysis, in Plexon Offline Sorter, and exported to text files for analysis in MATLAB (Mathworks, Nantick, MA). Low-SNR multi-unit activity is defined here as threshold crossings without a distinct action potential shape which still correlate with an input stimulus. These were detected using a custom MATLAB script with a per-channel threshold set at ±3 times root-mean square (RMS) of the high-pass filtered neural data. Neural data statistics were calculated with JMP (SAS Institute Inc., Cary, NC). Aggregate action potential characteristics were calculated for each unit, including peak-to-valley amplitude and signal-to-noise ratio. Because many of the *Aplysia* trials were contaminated with stimulation artifact and large high-density neural spiking, noise used to characterize SNR was calculated from the median of the raw signal amplitude rather than RMS, as shown in Equation 1 (the expression being multiplied is an estimate of the standard deviation of the background noise, where x is the 250 Hz high-pass filtered signal including stimulation artifact and spikes, and 0.6745 is an empirical correction) [52].

$$Noise = 3 * median\left\{\frac{|x|}{0.6745}\right\} \quad (1)$$

For feline single units, SNR for single- and multi-unit activity was calculated as the ratio of mean peak-to-peak amplitude of the sorted waveform to 3 times the root mean square (RMS) of the noise (filtered signal with unit regions removed). When neural activity was elicited by sensory stimulus, firing rates were calculated using a custom MATLAB script every 0.5 s with a 1 s triangular kernel, and rate was correlated to the stimulus. Due to the high density of our electrode sites, units were often recorded simultaneously on several channels. An unsupervised consensus clustering algorithm developed by Bruno et al. was used to group units by putative source, and detected clusters with identical or similar activity were manually combined [53]. This gave an efficient way to associate the units firing across multiple channels and consider them in aggregate. The spatial extent of these clusters was calculated by multiplying the vertical and horizontal spatial range of active electrodes.

Because the relationship between stimulus and neural firing rates is expected to be monotonic but not necessarily linear (and in the case of bladder pressure, has been shown to have a distinctly non-linear hysteresis [21]), the Spearman correlation coefficient was calculated to determine the strength of the relationship [54]. The brushing, catheter sliding, and joint-bending stimuli in feline experiments were modeled as binary signals corresponding to on/off periods for correlation. Bladder pressure was correlated with neural firing rate directly. When possible, highly significant and convincingly correlated activity ($R > 0.7$ for non-bladder trials, $R > 0.5$ for bladder trials, $p < 0.01$, visually similar) was mapped back to the location on the DRG from where it was recorded to start building a somatotopic map. The cutoff value was chosen to be higher than the correlation of an input stimulus with a baseline recording.

In some feline trials, simultaneous spikes from a presumed single neuron were observed on multiple closely-spaced channels. To demonstrate the potential of the GSEA for neuronal mapping, a technique from Lee et al. 2007 was used to estimate neuron source location from features of the simultaneously detected waveforms [55]. The method models the neuron source as a single point located in Cartesian space relative to a tetrode. Equation (2) describes the relationship of the potential V(t) detected at the electrode with the unknown actual source current I(t), the assumed homogeneous conductivity of the medium sigma (σ), and the distance of the neuronal source from the electrode $r_i(x,y,z)$, where (x,y,z) are the three unknown coordinates of the source location:

$$V(t) = \frac{I(t)}{4\pi\sigma * r_i(x, y, z)} \quad (2)$$

Four known values of V(t) must be used to solve this equation's four unknown values. Essentially, the distance from each electrode to the neural source is calculated, and the intersection of these distances is the location estimate. The mean peak voltage of the detected spike on each electrode was used as the feature for calculation, as this is assumed to be most representative of soma firing. No estimate of σ is necessary aside from the assumption of homogeneity, as it cancels out in the final calculation. More details of the linear algebra used for this estimation can be found in Lee et al. 2007 [55]. In some cases, the spikes were detected on a pentrode (5 electrodes), which gave four sets of tetrodes (4 electrodes) for estimation of the source location. In these cases, the mean of the four estimates was used to estimate location, with the standard deviation of each coordinate used to give a sense of the error. Note that since these estimates are not independent, their standard deviation cannot be relied on mathematically, only as an estimate. Additionally, the algorithm used fails if all electrodes are co-planar. To resolve this issue, one of the electrodes in each pentrode used for calculation was assumed to be slightly out of plane on a spherical surface with radius 100–2500 μm, with real solutions below the electrodes considered to be potentially valid estimates. Increasing radius of curvature gives a "flatter" pentrode. Based on surgical measurements and publications, we assumed the range of S2, S1, and L7 DRG radii are 400±200, 630±200, and 800±200 um respectively, and that the GSEA conforms within this range even if the surface bending is not perfectly conformal [30]. Our estimated range leaves room for slightly larger or smaller curvature.

Results

Invertebrate Results

In total, recordings were attempted in eighteen healthy isolated *Aplysia* buccal ganglia. After several unsuccessful attempts to obtain recordings without altering the ganglia sheath, it became clear that sheath thinning would be necessary to obtain neural recording. Sheath thinning was carried out successfully in seven *Aplysia* ganglia, of which four yielded action potential recordings. This is a much higher success rate than only one of eleven non-thinned ganglia yielding recordings. In total, we report five *Aplysia* ganglia yielding sortable single-unit action potentials (on at least one electrode channel following stimulation of the buccal

nerve). The mean number of channels active in successful trials was 19 (range 1–53), and the mean number of units on an active channel was 2.1, with a standard deviation of 1.5 and a maximum of 8. The median peak-to-peak voltage observed was 66.3 μV, and the largest unit had a mean magnitude of 713.0 μV. Noise on active channels had a mean value of 19.4 μV, leading to an SNR ranging from 1.16 to 30.3, with a median of 3.5.

In all but one experiment, individual units were observable on multiple channels. One trial from each experiment was analyzed to summarize the properties of this spatial oversampling. The magnitude of the same unit on different channels varied, with a median ratio of large-channel amplitude to small-channel amplitude of 3.64 (range: 1.38–16.38). The number of channels a single unit appeared on ranged from 2 up to 29, with a spatial range of up to 0.41 mm^2 (median: 0.08 mm^2). For reference, the active surface area of the array was 0.47 mm^2, and the largest cell bodies in *Aplysia* ganglia have a projected surface area of 0.79 mm^2 (1 mm diameter), though most are somewhat smaller (down to 7 μm in diameter, or 38 μm^2 [56].

Figure 2 shows the array on the buccal ganglia, a sample trial with spatially oversampled units, and sample waveforms with raw voltage traces and raster plots.

Feline Results

A total of eight cats were used in this study (six male, two female, age: 10–15 months old, 3.9–5.5 kg). In six of eight experiments, we were able to detect single- and/or multi-unit neural activity from one or several DRG, including L7, S1, and S2. Multi-unit activity, defined here as threshold crossings not separable as single units but still correlated with an applied stimulus was observed in two experiments that also had single units and in three additional experiments for a total of five. In some cases, both single and multi-units were observed during the same trials. Multi-unit activity was observed in response to tail brushing (3 experiments/3 attempted, successful on both S1 and S2), scrotum/genital brushing (1/2, on S2), anal brushing (2/4, on S2), leg brushing (3/7, on L7 and S2), ankle flexion (1/2, on L7), and bladder pressure (1/5, on S2). The neural activity correlation with input was similar for all stimulation types, with a mean of 0.76 and a standard deviation of 0.04. The mean number of active multi-unit channels was 28.5, with a range of 1 to 62. These results are summarized by experiment in Table 1, with “Successful Placement” referring to the number of locations at which the GSEA recorded either single- or multi- unit activity. “Active Channels” are calculated on a per trial basis, while the other columns are calculated for each active channel in the experiment. Mean SNR is nearly identical for all multi-unit activity because the threshold for events is set relative to the noise. Figure 3 shows samples of this multi-unit activity in response to either dermatome brushing or bladder pressure, as well as an array map of this activity and an observed somatotopy of the S1 and S2 DRG from recordings in one experiment.

In experiment 6, multiple placements on two neighboring DRG (left side) all yielded multi-unit activity significantly correlated with sensory input, including anal brushing (max correlation: R=0.79), tail brushing (max correlation: R=0.77), and bladder pressure (max correlation: R=0.85) (Fig. 3D). In this experiment, different stimuli elicited neural activity in different regions of the DRG. Specifically, anal brushing and bladder pressure correlated

activity were observed only on the medial region of the S2 DRG, while tail brushing correlated activity was observed on the distal region of the S1 DRG and across the entire S2 DRG.

Single units were elicited in three experiments (1, 5, and 7), with an average of 12.5 ± 10 units per trial on 15 ± 8 channels (out of 64). Sortable single-units ranged in amplitude from 17.3 μV to 158.7 μV, with SNR ranging from 1.1 to 7.3 (observed peak-to-peak noise 31 ± 16 μV). These units were elicited on L7 from joint bending (1 experiment with single units/2 attempted), on L7 from leg brushing (2/7), and on S1 or S2 from tail, anal, or genital brushing (1/5). In one experiment, single units were observed in response to changes in bladder pressure (1/5). The units were observed on a tetrode of sites spaced 30 μm from each other. Correlation of this unit with bladder pressure ranged from 0.49 to 0.61. Though this unit was oversampled on a tetrode, source localization estimates did not converge.

In 5 trials during experiment 1, single units were observed on five pentrodes (five electrodes with 25 μm pitch), allowing for source localization calculations. In 3 of these trials, this activity was detected on two pentrodes. The range of pentrode curvatures for a realistic source location estimate (real and below the electrode plane) was 100 to 2500 μm. In every case the estimated distance of the neural source increased with increasing estimates of the radius of curvature (flatter pentrode). Standard deviation of the estimated location also increased with curvature, but the rate of change of estimates decreased with curvature. For example, the difference between estimated location for 100 μm and 250 μm was always larger than the difference between 500 μm and 1000 μm. Assuming the flattest curvature in each case, neural sources were detected with estimated depths of 25 ± 1 μm to 107 ± 14 μm and estimated normal distances from pentrode center of 3.8 ± 1 μm to 135 ± 44 μm. Figure 4 shows the units detected in one of these experiments as well as an estimate of the source location of this unit.

In two experiments (3 and 7), electrical stimulation was applied to sacral DRG through the GSEA. In experiment 3, the right S1 DRG was stimulated. Single-channel stimulation yielded a tail twitch response at a threshold of 300 μA, though this was not present on every channel. With half (32) of the channels stimulated (the maximum for that array connector configuration), the threshold for tail twitching was 22.5 μA. In the second experiment, the GSEA was positioned on left S2. Stimulating on all channels, the threshold for tail-twitching was 45 μA. Stimulating on half (32) or a quarter (16) of the channels, the threshold was 60 μA. The 4-channel threshold was 90 μA, the 2 channel threshold was 120 μA. Rough regional trends in response to stimulation were observed, and stimulating channels as close as 250 μm apart yielded different motor responses (tail-twitching or no response).

Raw and analyzed data, and MATLAB scripts used in data analysis can be found online at [57].

Discussion

In this pilot study of a novel electrode designed specifically for surface-based interface with neural ganglia, we have demonstrated the ability of a flexible thin-film multi-electrode array

to both record and stimulate neural activity in invertebrate ganglia (Fig. 2) and feline DRG (Fig. 3 & 4). Single units detected in *Aplysia* buccal ganglia were often observed on multiple channels simultaneously and had recorded amplitudes of up to 713 μV and typical SNR of 2.63. Single units detected on feline DRG were also observed on multiple channels simultaneously. These single units were often correlated with brushing of associated dermatome areas or joint flexion. In cases when single units were observed on five closely-spaced electrode sites, we used a source localization algorithm to predict the depth of recorded neurons up to 107 μm (Fig. 4). We also observed DRG multi-unit activity correlated with dermatome brushing and bladder pressure. In one experiment, data from multiple array placements on multiple DRG allowed for simple somatotopy mapping of neural responses to several different types of sensory stimuli, including dermatome brushing and bladder pressure (Fig. 3D).

Neural activity was observed in six of eight feline experiments. The two experiments in which no DRG surface recordings were observed were all terminal experiments at the end of chronic implant periods for other objectives [8]. It is possible that a general increase in scar tissue in the region contributed to a lack of results in those procedures.

Previous studies have reported recording from the surface of invertebrate buccal ganglia using glass MEA [44], [45], [58]. These studies were also able to record single-unit activity, with multiple units on single channels and oversampling of units on multiple channels as demonstrated here. While our largest unit (~700 μV) was somewhat bigger than those reported in the previous work (200–300 μV), the typical waveforms were similar in size. A disadvantage of the glass MEA was the need to compress the ganglia against the surface, which by mechanically deforming the neurons could change the native firing characteristics. The GSEA also has the potential to be used in intact buccal mass preparations to study neural network activity together with muscle activity, which would be impossible with a stiff glass MEA [59].

Gaunt et al. (2011) reported single- and multi-unit neural activity recorded from the surface of feline lumbar DRG related to hind limb movement. Our study successfully built on these previous findings by widening the scope of sensory inputs recorded using the surface array. The largest reported unit had a peak-to-peak magnitude of about 200 μV and SNR of 8.1, which compares favorably with the largest feline unit reported here (magnitude 158 μV, SNR 7.3). While noise was not quantified, the noise in Gaunt et al. appeared to have a peak-to-peak magnitude of between 20 μV and 30 μV, which aligns with the average value of 31 μV observed in this study. Gaunt et al. reported a superior average yield (% active channels) of single unit activity, between 30% and 40% depending on the type of electrode used compared to our average of 23% yield. However, the electrode arrays used in Gaunt et al. had only 16 or 32 electrodes per array, so our 64-channel arrays of similar footprint actually had a greater number of detected single-units. In terms of multi-unit activity, the GSEA had a mean yield in successful trials of 41%, which is slightly lower than but still comparable to the ~45% reported by Gaunt et al. (not calculated in that study, but estimated based on reported active channel yield and multi-unit/single-unit ratio). The arrays discussed in Gaunt et al. consistently required downward pressure on the array to detect neural signals. While

we occasionally used this technique in our research, it was not a necessity in most cases. This represents an improvement in our design [39].

Other than Gaunt et al., observations of single units from surface-based neural recordings with flexible electrode arrays have rarely been previously reported, regardless of target neural location. The only example is Khodagholy et al., who described NeuroGrid, an electrode technology similar to the GSEA but designed for use on the surface of the brain (either neocortex or hippocampus) [60]. While comparison to this study is limited by the differing application, it is worth noting that the maximum single-unit spike amplitude observed by Khodagholy et al. was approximately 100 μV, comparable to our maximum of 158 μV. Observed RMS noise in their study was 8 μV, which is roughly a peak-to-peak value of 23 μV, slightly lower but still comparable to the 31 μV level in our study. Their noise measurement was taken postmortem, however, which eliminates background biological noise [60].

Other groups have also adapted thin-film technologies for nerve interfacing in peripheral locations. The flexible split ring electrode, presented by Lee et al., is a flat polyimide annulus with gold/platinum electrodes on the inner region to make contact with the nerve. The ring splits at the top to accommodate placement around a nerve, and the inner electrodes bend to make good contact with the nerve surface. In an acute study, this electrode array was demonstrated to evoke compound muscle action potentials and record compound nerve action potentials from the sciatic nerve in rats. This configuration partially solves the problem of attaching a thin film to a nerve, and could hypothetically be adapted for use in DRG with proper sizing and careful surgical technique per the constraints discussed previously [61]. Future implementations of our device could utilize a passive thin-film split ring design to secure the device to the distal and proximal spinal root, with the electrode array remaining on the DRG itself.

A more straight-forward design by Caravaca et al. consisted of a parylene array with a row of tungsten-titanium electrodes of different sizes, both larger and smaller than the sites in this study. This array was demonstrated acutely on the mouse vagus nerve, folded around the nerve to record compound action potentials in response to chemical stimuli. Recording noise was not quantified, but it was reported that the very small sites (225 μm^2) had impedance too high for recording above the noise floor. While chronic recordings were not reported, histology of 12 week chronic implants suggested limited inflammation around the array [62]. Similarly, Diaz-Butia et al. demonstrated an array of amorphous silicon-carbide insulation with conductive silicon-carbide electrode sites on polyimide backing. This flexible array was shown to record compound action potentials and μ-ECoG on rat sciatic nerve and cortex, respectively [63]. Either of these designs were similar enough to the GSEA to be possibly used on the DRG with similar results.

The primary issue with the use of flexible arrays to record from DRG in this study is the general difficulty of successful and repeatable implant, because of the surgical environment and array properties. Vertebral bone is highly vascularized, and laminectomy can cause bleeding into the implant area. Slow blood pooling impedes visibility of the DRG, making it difficult to place the array and visualize it once in place. The arrays also float on top of the

liquid, lifting them from the DRG surface. Bleeding can be controlled to a certain extent with bone wax, absorbent materials, clotting aids, and suction, but each of these have limitations in terms of effectiveness and maintaining visibility of the implant area. Bleeding was highly variable across our experiments, and was often a strong predictor of success or failure of the neural interface. Similar implantation challenges would likely be faced by the electrode designs of Caravaca and Diaz-Butia discussed above. The successful application of surface arrays in the brain were likely aided by the lack of significant blood pooling [60]. Vertebral bleeding also occurs for use of DRG-penetrating arrays, though these designs are placed more quickly and secure themselves to the tissue.

The arrays were also difficult to use due to the thin profile and material properties intended to make them superior to penetrating arrays in function. The thin polyimide was difficult to manipulate using forceps without tearing, and so most array placement involved placing the array on a moist surface near the interface target and then sliding it over the DRG of interest. There is a clear tradeoff between device thickness and robust handling. We preferred 4.4-μm thick substrates, but also tested a 3.6-μm thick device and found it more conformal but more easily kinked. Previously, polyimide has been made as thin as 2.5 μm but required a temporary silk coating to manage placement of the recording array [49]. Our concern was this technique would only work here if we could keep the surface dry and quickly secure the array in an accurate position with a microsuture or adhesive. As seen in Fig. 1D, the conformal nature of this material and thickness was good for relatively large DRG, but not ideal. The surface tension of the very light, flexible arrays interacting with fluids will dominate any similar array and even more so for thinner structures. The thinness and weight of the array also made it vulnerable to small air currents and static electricity. We attempted to address this issue by placing Silastic® tubing (DOW Corning, Midland, MI) around most of the array ribbon length to add weight, which worked but came at the expense of array maneuverability. This difficulty in handling was exacerbated by the small size of the target. Feline sacral-level DRG in surgery have an exposed surface area on the order of 0.5–1 mm^2, giving little margin for error in placement. To use these arrays as a tool for mapping the DRG would require the ability to place the array in a repeatable position or positions, which was not possible within the scope of this study. Even with these challenges, through this pilot study we were able to observe a range of neural signals.

We have demonstrated that this type of array, once placed, can successfully record and stimulate neural activity in acute procedures. No method of securing the array was used in any recording, with the exception of some natural fluid thickening around the array that held it in place against light tugging. This is not a problem unique to surface recording, as penetrating arrays in the DRG must have connection wires secured with suture or handled delicately to stay in place in the tissue [8]. A variety of one-off attempts were made to more permanently maintain array position, including application of quick setting elastomers (Kwik-sil™ or Kwik-cast™ (World Precision Instruments, Sarasota, FL)), and cyanoacrylates (Super Glue®-like compounds), both alone and in combination. None of these materials secured the array against the kind of forces that would be experienced in a chronic implant. Further, while recording was attempted after application of these chemicals, no neural activity was ever observed. It is possible that the compounds seeped between the electrode and the tissue surface, blocking conduction. Future design iterations may include

eyelets suitable for suturing the array to nearby tissue, such as the spinal cord itself. Khodagholy et al. reported implanting their array stably for 10 days in a rat, with single-units maintaining both amplitude and channel location. The study did not report using any kind of adhesive or suture to maintain array position [60]. However, skull-mounted brain implants are subject to much less motion than would be a chronic spinal root implant.

During the course of this study, we evaluated a number of different electrode layouts (Fig. 1D). While the number of experiments with each layout was not sufficient to undertake a formal analysis, we can make a few observations. The GSEAs tested had a range of electrode pitch from 25 μm to just over 1 mm. In the *Aplysia* experiments, the spatial range of single-unit recording on multiple channels covered about 87% of the active array area. In felines, however, single-units were oversampled only on channels with separation smaller than 35 μm, representing a spatial extent of 900 μm^2 or 0.16% of the active array area of 0.56 mm^2. This is a direct result of differences in cell body size, with the largest feline DRG cell bodies (diameter ~80 μm) hugely dwarfed by the largest *Aplysia* cell bodies (diameter 1 mm) [31], [56]. Related multi-unit activity in felines had a significantly larger spatial extent, up to 100% of the array, so a large active array area also has advantages. This suggests that for vertebrate GSEAs, there should be a balance between maximizing active array area to cover the entire DRG and having sites <35 μm apart to oversample units. Spatial oversampling provides advantages for improved accuracy in spike sorting and for neural source localization, as demonstrated in this study [64], [65].

Future work in *Aplysia* will include simultaneously recording with the GSEA and nerve suction electrodes to establish ground truth validation of which cells are being activated [50]. Further, the GSEA could be used as a mapping tool in an intact preparation of *Aplysia* which includes electromyogram recordings of the buccal mass muscles [59]. It would also be feasible to fabricate an array sized, shaped, and laid out specifically for buccal ganglia recordings, to sample from the entire ganglia or focus on regions of interest to *Aplysia* researchers.

The primary goal of this study, however, was to produce a surface array for acute recording from the surface region of vertebrate DRG. Future work in felines will include performing chronic implants, taking advantage of the less invasive surface-based approach to potentially improve recording life by reducing immune and scarring responses. This potential benefit will depend on whether tissue in-growth occurs under the array, as has been observed for ECoG arrays, as well as the ability of the array to survive sterilization and long-term implant without delamination [66]. We will also interface with other spinal levels, explore microstimulation further, and continue to investigate electrode geometries. Computational modeling studies will improve our understanding of this interface and suggest design improvements, especially as regards electrical coupling between the GSEA and the epineurium-sheathed tissue. To further leverage the density of our electrode sites, we will use advanced sorting techniques designed for high-density electrode arrays such as those proposed by Jun et al. for their MATLAB JRClust system [67]. We will also perform experiments to validate the proposed source-localization.

Conclusion

We have demonstrated for the first time the ability of a conformable polymer electrode array to record neural signals from the surface of ganglia of different types. We demonstrated the capability of this array to record single-unit action potentials from the surface of *Aplysia californica* buccal ganglia, and the possibility of using the array to map activity throughout the structure. We used this array in acute feline experiments to detect both single- and multi-unit neural activity related to manual stimulation of cutaneous afferents and bladder pressure. We also showed that this type of array could potentially be used to map the sources of neural signals in the DRG with a source localization algorithm. Refinement of the array and handling procedures will allow for repeatable and securable placement and will be necessary before it can be used as a long-term interface. However, because a non-penetrating surface-based approach has significant advantages, not only for neural recording in general but for the specific morphology of the DRG, this approach may have better chronic performance than penetrating arrays.

Acknowledgments

This work was a collaboration between the Bruns Peripheral Neural Engineering and Urodynamics Laboratory (pNEURO Lab), the Yoon Lab, and the Chiel Lab. The authors would therefore like to thank the members of those laboratories for support and advice in designing, fabricating, and testing the surface array. In particular, we acknowledge Aileen Ouyang, Ahmad Jiman, Lauren Zimmerman, Shani Ross, Henry Hilow, Nicholas Peck-Dimit, John Bentley, Catherine Kehl, Hui Lu, and Fan Wu. Research reported in this publication was supported by the Craig H. Neilsen Foundation (Grant # 314980), the National Institute of Biomedical Imaging and Bioengineering of the National Institutes of Health (SPARC program Award # U18EB021760), the Michigan Institute for Clinical & Health Research, which is funded by the National Center for Advancing Translational Studies of the National Institutes of Health (Grant #'s UL1TR000433 and UL1TR002240), and Seed Funding for Innovative Projects in Neuroscience from the Michigan Brain Initiative Working Group (MiBrain). The content is solely the responsibility of the authors and does not necessarily represent the official views of the Craig H. Neilsen Foundation, the National Institutes of Health, or the University of Michigan.

References

1. Aoyagi Y, Stein RB, Branner A, Pearson KG, Normann RA. Capabilities of a penetrating microelectrode array for recording single units in dorsal root ganglia of the cat. J Neurosci. Methods. 2003; 128:9–20. [PubMed: 12948544]
2. Bruns TM, Gaunt RA, Weber DJ. Multielectrode array recordings of bladder and perineal primary afferent activity from the sacral dorsal root ganglia. J Neural Eng. Oct.2011 8(5):56010.
3. Bruns TM, Wagenaar JB, Bauman MJ, Gaunt RA, Weber DJ. Real-time control of hind limb functional electrical stimulation using feedback from dorsal root ganglia recordings. J Neural Eng. 2013; 10(2):1–13.
4. Weber DJ, Stein RB, Everaert DG, Prochazka A. Decoding sensory feedback from firing rates of afferent ensembles recorded in cat dorsal root ganglia in normal locomotion. IEEE Trans. Neural Syst. Rehabil. Eng. 2006; 14(2):240–243. [PubMed: 16792303]
5. Stein RB, Weber DJ, Aoyagi Y, Prochazka A, Wagenaar JBM, Shoham S, Normann RA. Coding of position by simultaneously recorded sensory neurones in the cat dorsal root ganglion. J Physiol. 2004; 560(3):883–896. [PubMed: 15331686]
6. Holinski BJ, Everaert DG, Mushahwar VK, Stein RB. Real-time control of walking using recordings from dorsal root ganglia. J Neural Eng. 2013; 10(5):56008.
7. Umeda T, Seki K, Sato M, Nishimura Y, Kawato M, Isa T. Population Coding of Forelimb Joint Kinematics by Peripheral Afferents in Monkeys. PLoS One. 2012; 7(10):1–15.

8. Khurram A, Ross SE, Sperry ZJ, Ouyang A, Stephan C, Jiman A, Bruns TM. Chronic monitoring of lower urinary tract activity via a sacral dorsal root ganglia interface. J Neural Eng. 2017; 14(3): 36027.
9. Snellings AE, Yoo PB, Grill WM. Urethral flow-responsive afferents in the cat sacral dorsal root ganglia. Neurosci. Lett. 2012; 516(1):34–38. [PubMed: 22480694]
10. NSCISC. Spinal Cord Injury Facts and Figures at a Glance. Natl. Spinal Cord Inj. Stat. Center, Birmingham, Alabama. 2016
11. Anderson KD. Targeting recovery: priorities of the spinal cord-injured population. J Neurotrauma. 2004; 21(10):1371–1383. [PubMed: 15672628]
12. Collinger JL, Boninger ML, Bruns TM, Curley K, Wang W, Weber DJ. Functional Priorities, Assistive Technology, and Brain-Computer Interfaces after Spinal Cord Injury. J Rehabil Res Dev. 2014; 50(2):145–160.
13. Hamid S, Hayek R. Role of electrical stimulation for rehabilitation and regeneration after spinal cord injury: An overview. Eur. Spine J. 2008; 17(9):1256–1269. [PubMed: 18677518]
14. Van Den Brand R, Heutschi J, Barraud Q, van den Brand R, DiGiovanna J, Bartholdi K, Huerlimann M, Friedli L, Vollenweider I, Moraud EM, Duis S, Dominici N, Micera S, Musienko P, Courtine G. Restoring voluntary control of locomotion after paralyzing spinal cord injury. Science. 2012; 336(6085):1182–5. [PubMed: 22654062]
15. Collinger JL, Foldes S, Bruns TM, Wodlinger B, Gaunt R, Weber DJ. Neuroprosthetic technology for individuals with spinal cord injury. J Spinal Cord Med. 2013; 36(4):258–272. [PubMed: 23820142]
16. Gaunt RA, Hokanson JA, Weber DJ. Microstimulation of primary afferent neurons in the L7 dorsal root ganglia using multielectrode arrays in anesthetized cats: thresholds and recruitment properties. J Neural Eng. 2009; 6(5):55009.
17. Hokanson, JA., Ayers, CA., Gaunt, RA., Bruns, TM., Weber, DJ. Effects of spatial and temporal parameters of primary afferent microstimulation on neural responses evoked in primary somatosensory cortex of an anesthetized cat; 33rd Annual International Conference of the IEEE Engineering in Medicine and Biology Society; 2011. p. 7533-7536.
18. Fisher LE, Ayers CA, Ciollaro M, Ventura V, Weber DJ, Gaunt RA. Chronic recruitment of primary afferent neurons by microstimulation in the feline dorsal root ganglia. J Neural Eng. 2014; 11(3):36007.
19. Ayers CA, Fisher LE, Gaunt RA, Weber DJ. Microstimulation of the lumbar DRG recruits primary afferent neurons in localized regions of lower limb. J Neurophysiol. 2016; 116(1):51–60. [PubMed: 27052583]
20. Bruns TM, Weber DJ, Gaunt RA. Microstimulation of afferents in the sacral dorsal root ganglia can evoke reflex bladder activity. Neurourol. Urodyn. 2014; 34(September 2013):65–71. [PubMed: 24464833]
21. Ross SE, Sperry ZJ, Mahar CM, Bruns TM. Hysteretic behavior of bladder afferent neurons in response to changes in bladder pressure. BMC Neurosci. 2016; 17(57):1–12. [PubMed: 26728069]
22. Patil AC, Thakor NV. Implantable neurotechnologies: a review of micro- and nanoelectrodes for neural recording. Med. Biol. Eng. Comput. 2016; 54(1):23–44. [PubMed: 26753777]
23. Tyler DJ, Durand DM. Functionally selective peripheral nerve stimulation with a flat interface nerve electrode. IEEE Trans. Neural Syst. Rehabil. Eng. 2002; 10(4):294–303. [PubMed: 12611367]
24. Perez-Orive J, Durand DM. Modeling study of peripheral nerve recording selectivity. IEEE Trans. Rehabil. Eng. 2000; 8(3):320–329. [PubMed: 11001512]
25. Durand DM. Selective Fascicular Recording of the Hypoglossal Nerve Using a Multi- Contact Nerve Cuff Electrode. Image (Rochester, N.Y.). 2003:2172–2175.
26. Prochazka A, Gorassini M. Models of ensemble firing of muscle spindle afferents recorded during normal locomotion in cats. J Physiol. 1998; 507(1):277–291. [PubMed: 9490851]
27. Edell DJ, Van Toi V, McNeil VM, Clark LD. Factors Influencing the Biocompatibility of Insertable Silicon Microshafts in Cerebral Cortex. IEEE Trans. Biomed. Eng. 1992; 39(6):635–643. [PubMed: 1601445]

28. Polikov VS, Tresco PA, Reichert WM. Response of brain tissue to chronically implanted neural electrodes. J Neurosci. Methods. 2005; 148(1):1–18. [PubMed: 16198003]
29. Wark HAC, Mathews KS, Normann RA, Fernandez E. Behavioral and cellular consequences of high-electrode count Utah Arrays chronically implanted in rat sciatic nerve. J Neural Eng. 2014; 11(4):46027.
30. Ostrowski AK, Sperry ZJ, Kulik G, Bruns TM. Quantitative models of feline lumbosacral dorsal root ganglia cell density. Neurosci. Methods. 290:116–124.
31. Miletic V, Lu GW. Characteristics of action potentials recorded from cat spinal ganglion neurons in vivo. Brain Res. Bull. 1993; 31(5):531–538. [PubMed: 8495378]
32. Kim D-H, Viventi J, Amsden JJ, Xiao J, Vigeland L, Kim Y-S, Blanco Ja, Panilaitis B, Frechette ES, Contreras D, Kaplan DL, Omenetto FG, Huang Y, Hwang K-C, Zakin MR, Litt B, Rogers Ja. Dissolvable films of silk fibroin for ultrathin conformal bio-integrated electronics. Nat. Mater. 2010; 9(6):511–517. [PubMed: 20400953]
33. Minev IR, Musienko P, Hirsch A, Barraud Q, Wenger N, Moraud EM, Gandar J, Capogrosso M, Milekovic T, Asboth L, Torres RF, Vachicouras N, Liu Q, Pavlova N, Duis S, Larmagnac A, Vörös J, Micera S, Suo Z, Courtine G, Lacour SP. Electronic dura mater for long-term multimodal neural interfaces. Science (80-.). 2015; 347(6218):159–163.
34. Rodger DC, Fong AJ, Li W, Ameri H, Ahuja AK, Gutierrez C, Lavrov I, Zhong H, Menon PR, Meng E, Burdick JW, Roy RR, Edgerton VR, Weiland JD, Humayun MS, Tai YC. Flexible parylene-based multielectrode array technology for high-density neural stimulation and recording. Sensors Actuators, B Chem. 2008; 132(2):449–460.
35. Lawrence SM, Dhillon GS, Jensen W, Yoshida K, Horch KW. Acute peripheral nerve recording characteristics of polymer-based longitudinal intrafascicular electrodes. IEEE Trans. Neural Syst. Rehabil. Eng. 2004; 12(3):345–348. [PubMed: 15473197]
36. Boretius T, Badia J, Pascual-Font A, Schuettler M, Navarro X, Yoshida K, Stieglitz T. A transverse intrafascicular multichannel electrode (TIME) to interface with the peripheral nerve. Biosens. Bioelectron. Sep.2010 26(1):62–9. [PubMed: 20627510]
37. Lachapelle, JR., Bjune, CK., Kindle, AL., Czarnecki, A., Burns, JR., Grainger, JE., Segura, CA., Nugent, BD., Sriram, TS., Parks, PD. An implantable, designed-for-human-use peripheral nerve stimulation and recording system for advanced prosthetics; Engineering in Medicine and Biology Society (EMBC), 2016 IEEE 38th Annual International Conference of the; 2016. p. 1794-1797.
38. Rubehn B, Stieglitz T. In vitro evaluation of the long-term stability of polyimide as a material for neural implants. Biomaterials. 2010; 31(13):3449–3458. [PubMed: 20144477]
39. Gaunt, RA., Bruns, TM., Crammond, DJ., Tomycz, ND., Moossy, JJ., Weber, DJ. Single- and multi-unit activity recorded from the surface of the dorsal root ganglia with non-penetrating electrode arrays; Proc. Annu. Int. Conf. IEEE Eng. Med. Biol. Soc. EMBS; 2011. p. 6713-6716.
40. Ordonez J, Schuettler M, Boehler C, Boretius T, Stieglitz T. Thin films and microelectrode arrays for neuroprosthetics. MRS Bull. 2012; 37(6):590–598.
41. Cullins MJ, Chiel HJ. Electrode fabrication and implantation in Aplysia californica for multi-channel neural and muscular recordings in intact, freely behaving animals. J Vis. Exp. 2010; (40):e1791.
42. Duke AR, Jenkins MW, Lu H, McManus JM, Chiel HJ, Jansen ED. Transient and selective suppression of neural activity with infrared light. Sci. Rep. 2013; 3:2600. [PubMed: 24009039]
43. Lu H, Chestek CA, Shaw KM, Chiel HJ. Selective extracellular stimulation of individual neurons in ganglia. J Neural Eng. 2009; 5(3):287–309.
44. Novak JL, Wheeler BC. Recording from the Aplysia abdominal ganglion with a planar microelectrode array. IEEE Trans. Biomed. Eng. 1986; 33(2):196–202. [PubMed: 3007331]
45. Harris CA, Passaro PA, Kemenes I, Kemenes G, O'Shea M. Sensory driven multi-neuronal activity and associative learning monitored in an intact CNS on a multielectrode array. J Neurosci. Methods. 2010; 186(2):171–178. [PubMed: 19941897]
46. Yang J, Lu H, Kodama N, Feng T, Fernandez Galen R, Chiel HJ. Neural dynamics of a feeding pattern-generating circuit in the marine mollusk Aplysia californica. Society for Neuroscience 47th Annual Meeting. 2017

47. Hurwitz I, Neustadter D, Morton DW, Chiel HJ, Susswein AJ. Activity patterns of the B31/B32 pattern initiators innervating the I2 muscle of the buccal mass during normal feeding movements in Aplysia californica. J Neurophysiol. 1996; 75(4):1309–26. [PubMed: 8727380]
48. Ye H, Morton DW, Chiel HJ. Neuromechanics of multifunctionality during swallowing in Aplysia californica. J Neurosci. 2006; 26(5):1470–85. [PubMed: 16452671]
49. Morton DW, Chiel HJ. The timing of activity in motor neurons that produce radula movements distinguishes ingestion from rejection in Aplysia. J Comp. Physiol. A. 1993; 172(1):17–32. [PubMed: 8445578]
50. Lu H, McManus JM, Chiel HJ. Extracellularly identifying motor neurons for a muscle motor pool in Aplysia californica. J Vis Exp. 2013; 73(March):e50189.
51. Kuhn RA. Organization of Tactile Dermatomes in Cat and Monkey. J Neurophysiol. 1952; 16:169–182.
52. Quiroga RQ, Nadasdy Z, Ben-Shaul Y. Unsupervised Spike Detection and Sorting with Wavelets and Superparamagnetic Clustering. Neural Comput. 2004; 16(8):1661–1687. [PubMed: 15228749]
53. Bruno AM, Frost WN, Humphries MD. Modular deconstruction reveals the dynamical and physical building blocks of a locomotion motor program. Neuron. 2015; 86(1):304–318. [PubMed: 25819612]
54. Bonett DG, Wright TA. Sample size requirements for estimating Pearson, Kendall and Spearman correlations. Psychometrika. 2000; 65(1):23–28.
55. Lee CW, Dang H, Nenadic Z. An efficient algorithm for current source localization with tetrodes. Conf. Proc. IEEE Eng. Med. Biol. Soc. 2007; 2007:1282–1285. [PubMed: 18002197]
56. Zhao Y, Wang DO, Martin KC. Preparation of Aplysia sensory-motor neuronal cell cultures. J Vis. Exp. 2009; (28):7–9.
57. Peck-Dimit N, Sperry ZJ, Bruns TM. Flexible microelectrode array recordings from neural ganglia. Open Sci. Framew. 2018; doi: 10.17605/OSF.IO/68PU4
58. Gross GW. Simultaneous Single Unit Recording in vitro with a Photoetched Laser Deinsulated Gold Multimicroelectrode Surface. IEEE Trans. Biomed. Eng. 1979; BME-26(5):273–279.
59. McManus JM, Lu H, Chiel HJ. An in vitro preparation for eliciting and recording feeding motor programs with physiological movements in Aplysia californica. J Vis. Exp. 2012; (70):e4320. [PubMed: 23242322]
60. Khodagholy D, Gelinas JN, Thesen T, Doyle W, Devinsky O, Malliaras GG, Buzsáki G. NeuroGrid : recording action potentials from the surface of the brain. Nat. Neurosci. 2014; 18(2): 310–315. [PubMed: 25531570]
61. Lee S, Sheshadri S, Xiang Z, Delgado-Martinez I, Xue N, Sun T, Thakor NV, Yen SC, Lee C. Selective stimulation and neural recording on peripheral nerves using flexible split ring electrodes. Sensors Actuators, B Chem. 2017; 242:1165–1170.
62. Caravaca AS, Tsaava T, Goldman L, Silverman H, Riggott G, Chavan SS, Bouton C, Tracey KJ, Desimone R, Boyden ES, Sohal HS, Olofsson PS. A novel flexible cuff-like microelectrode for dual purpose, acute and chronic electrical interfacing with the mouse cervical vagus nerve. J Neural Eng. 2017; 14(6):66005.
63. Diaz-Botia CA, Luna LE, Neely RM, Chamanzar M, Carraro C, Carmena JM, Saves PN, Maboudian R, Maharbiz MM. A silicon carbide array for electrocorticography and peripheral nerve recording. J Neural Eng. 2017; 14:56006.
64. Gray CM, Maldonado PE, Wilson M, McNaughton B. Tetrodes markedly improve the reliability and yield of multiple single-unit isolation from multi-unit recordings in cat striate cortex. J Neurosci. Methods. 1995; 63(1–2):43–54. [PubMed: 8788047]
65. Lee, CW., Szymanska, Aa, Ikegaya, Y., Nenadic, Z. The accuracy and precision of signal source localization with tetrodes; Proc. Annu. Int. Conf. IEEE Eng. Med. Biol. Soc. EMBS; 2013. p. 531-534.
66. Schendel AA, Nonte MW, Vokoun C, Richner TJ, Brodnick SK, Atry F, Frye S, Bostrom P, Pashaie R, Thongpang S, Eliceiri KW, Williams JC. The effect of micro-ECoG substrate footprint on the meningeal tissue response. J Neural Eng. 2014; 11(4):46011.

67. Jun JJ, Mitelut C, Lai C, Gratiy SL, Anastassiou CA, Harris TD. Real-time spike sorting platform for high-density extracellular probes with ground-truth validation and drift correction. bioRxiv. 2017:1–29.

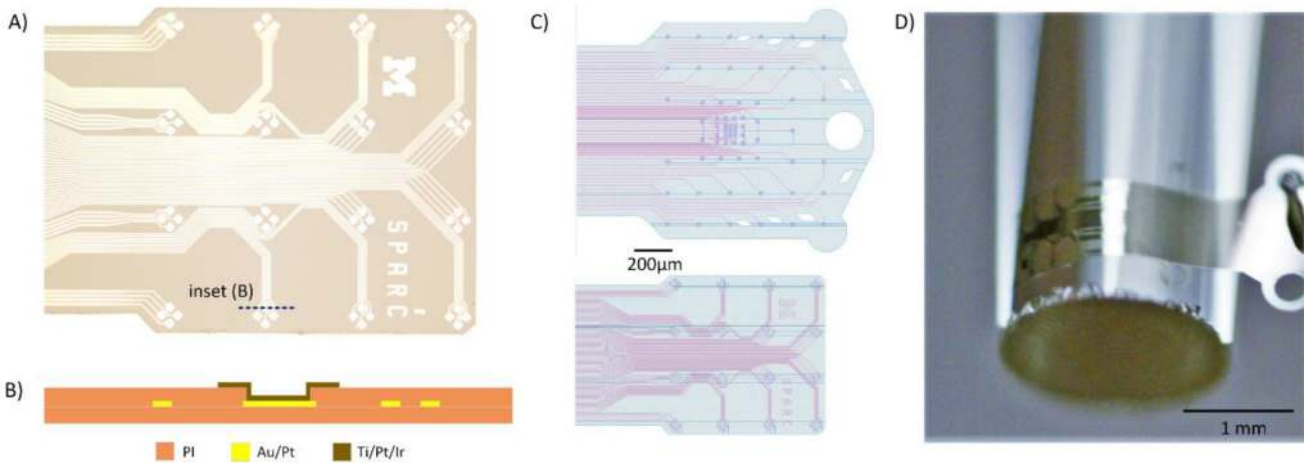

Figure 1.

A) Microscope image of a finished array. B) Fabrication stack diagram of electrode site (Ti/Pt/Ir) and traces (Au/Pt). C) Schematic layouts of tested arrays. D) Array curving to surface of 2 mm diameter rod.

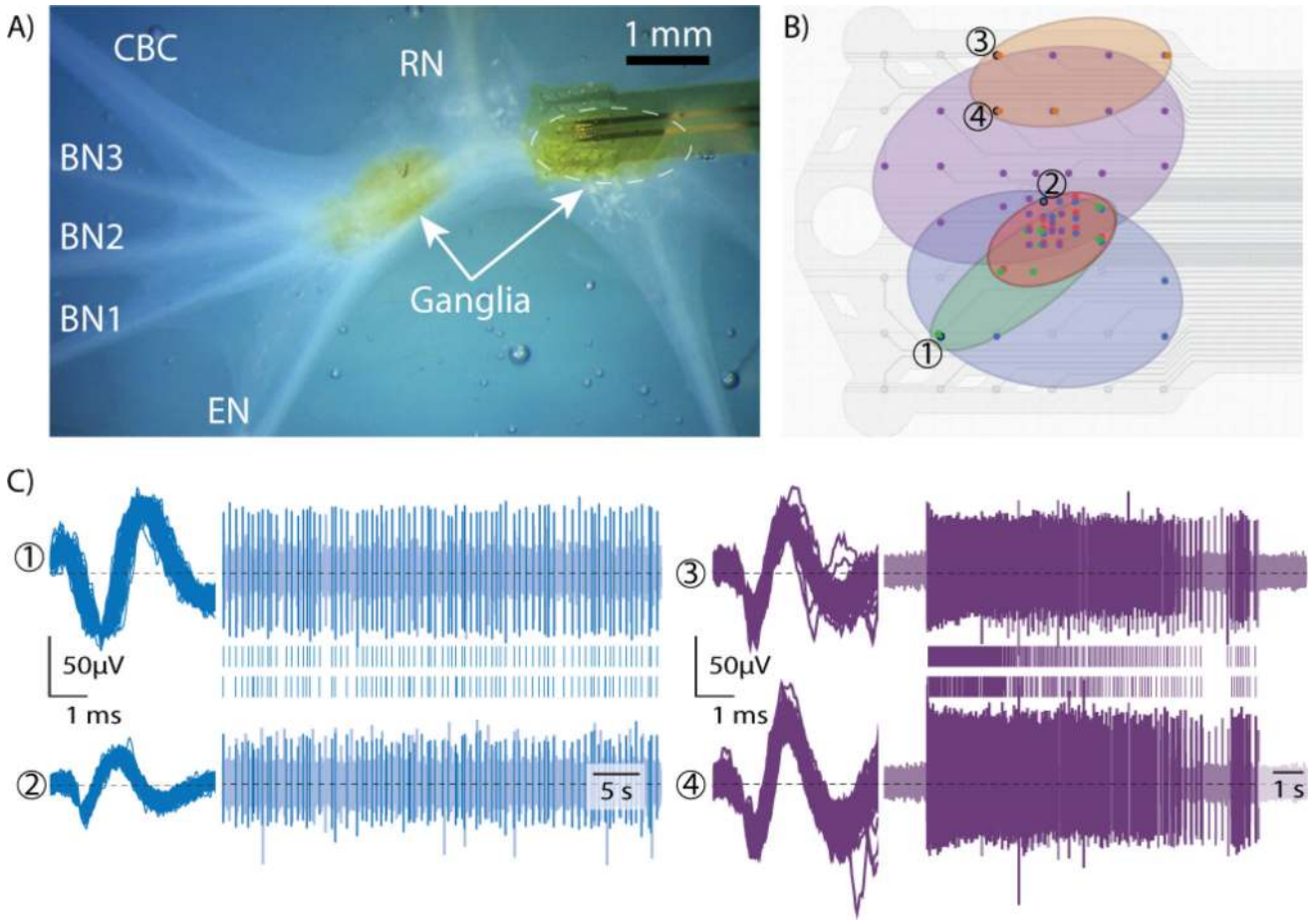

Figure 2.

A) Brightfield microscope image of array on buccal ganglia, with radular nerve (RN), buccal nerves (BN1-3), cerebral-buccal connective nerve (CBC), esophageal nerve (EN) and ganglia labeled (right ganglion obscured by array) B) Array schematic with 5 regions of similarly firing channel overlaid C) Sample waveforms, raw voltage traces, and raster plots [numbers and colors correspond to those in (B)] Note that the right (purple) unit is on channels with a second unit also recorded, which corresponded to the orange region

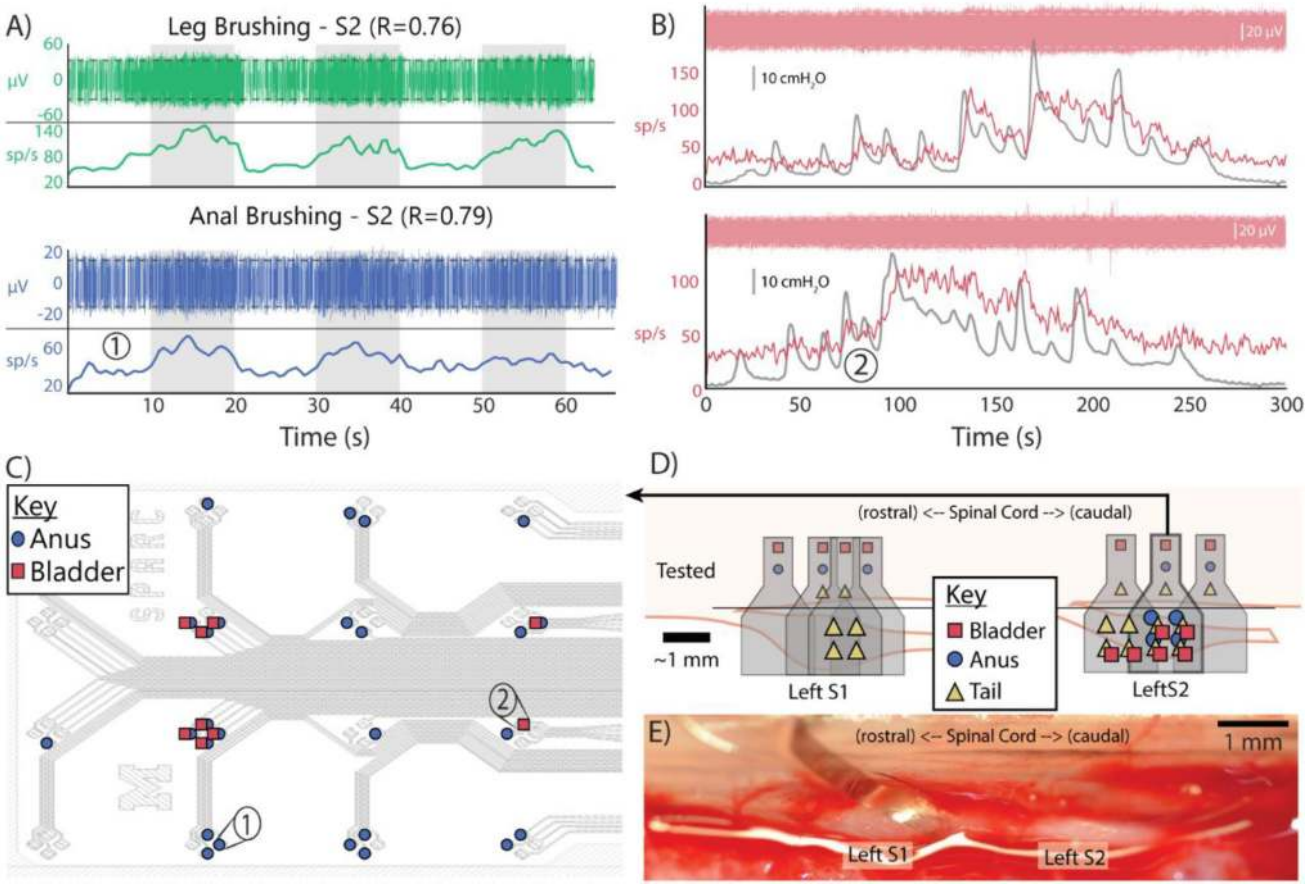

Figure 3.

A) Multi-unit activity recorded on S2 related to leg brushing in experiment 7 (top) and on S2 related to anal brushing in experiment 6 (bottom). Gray rectangles indicate periods of brushing. Titles indicate correlation. Red dashed lines indicate threshold for unit detection B) Multi-unit activity recorded on S2 related to bladder pressure in two trials of same experiment, including raw data, firing rate, and pressure trace. C) Array map of multi-unit activity from one experiment, indicating channels of bottom figures in (A) and (B). D) Map of detected multi-unit activity in one experiment on left S1 and S2. Gray shapes indicate approximate array locations. Colored shapes above black line indicate inputs tested at each array location. Colored shapes over the DRG indicate detected activity by array quartile. E) *In vivo* surgical image of array on caudal left S1.

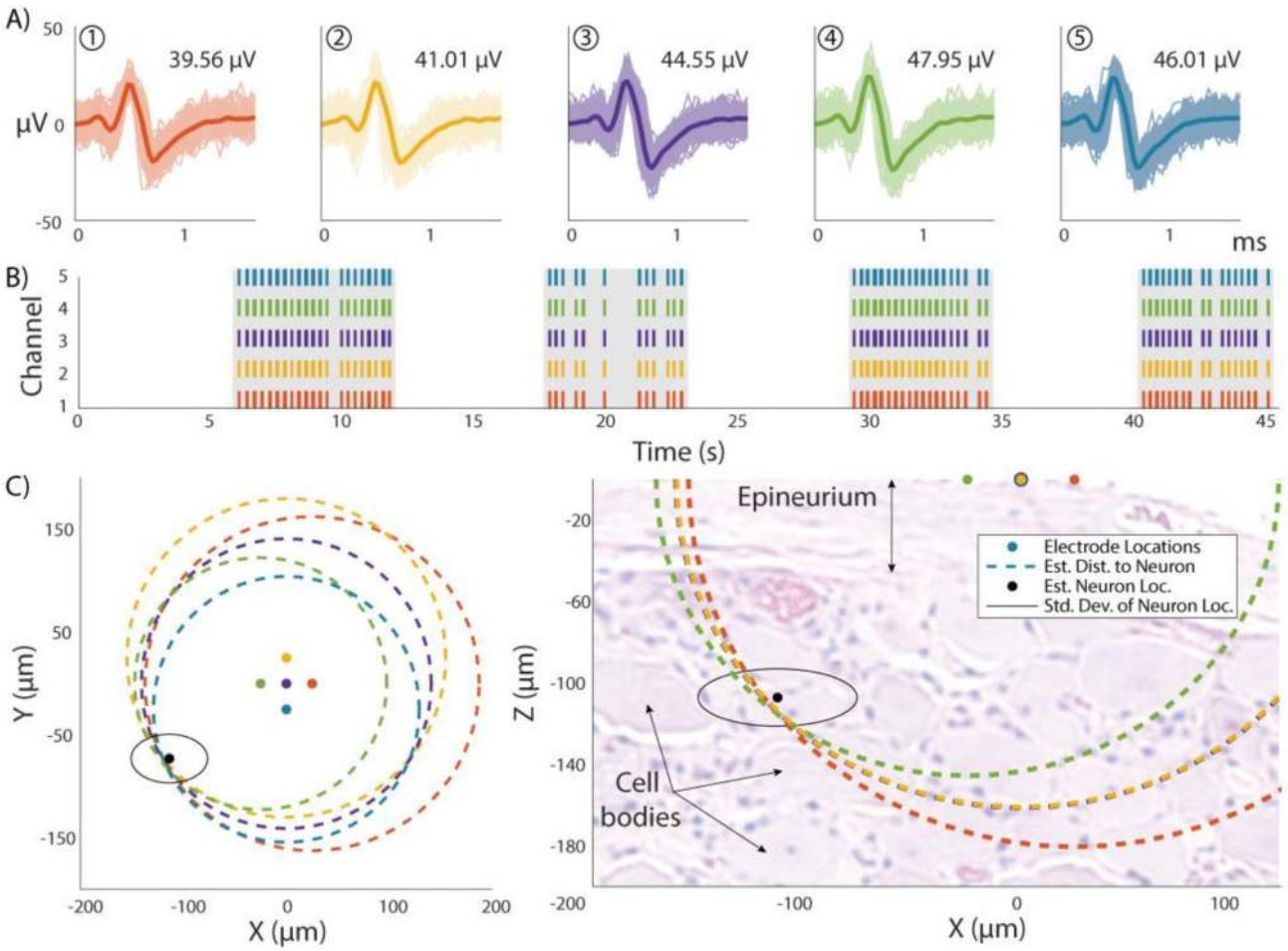

Figure 4.

A) Single unit detected simultaneously on 5 closely-spaced channels recorded from left L7 DRG responding to leg brushing. Waveforms shown color-coded by channel, with label indicating mean peak-to-peak waveform amplitude. Darker waveform is the mean waveform. B) Raster plot of waveforms in (A), showing simultaneity. Grey boxes indicate periods of leg brushing. (C) Estimate of neural source location. Dashed circles represent estimated distance of source from each electrode (colored circles), and their intersection (black circle) is the estimated source. The black line indicates the standard deviation of the estimate. The left plot is a top-down view through the array. The right plot is a side view axially through the DRG. A representative hematoxylin & eosin-stained DRG (from same experiment) is shown to scale in the side-view. The epineurium and some cell bodies are labeled for reference.

Table 1

Summary of data recorded from feline experiments with neural data

		Single-unit Activity			Multi-unit Activity		
Cat Expt	**Successful Placements**	**Active Channels**	**Mean Peak to Peak(μV)**	**Mean SNR**	**Active Channels**	**Mean Peak to Peak (μV)**	**Mean SNR**
1	2	11.9±3.9	31.1±9.9	3.5±1.1	26.8±4.8	20.1±2.7	1.1±0.0
4	1	-	-	-	39 (1 trial)	32.2±4.2	1.1±0.0
5	1	38 (1 trial)	40.7±6.0	*	-	-	-
6	3	-	-	-	34.7 ± 23.4	26.1±2.2	1.1±0.0
7	2	12.2±5.1	61.9±24.5	3.1±1.1	2.0 ± 1.4	49.3±12.4	1.1±0.0
8	2	-	-	-	26.3 ± 12.6	24.5±3.6	1.1±0.0

* raw data missing